RSC Advances

PAPER

View Article Online
View Journal | View Issue

Cite this: *RSC Adv.*, 2025, **15**, 10150

Catalytic application of a bimetallic–organic framework with phosphorus acid groups in the preparation of pyrido[2,3-*d*]pyrimidines *via* cooperative vinylogous anomeric-based oxidation†

Ali Reza Ataee-Najari,[a] Milad Mohammadi Rasooll,[a] Mahmoud Zarei,[*b] Mohammad Ali Zolfigol,[*a] Arash Ghorbani-Choghamarani[*a] and Mojtaba Hosseinifard[c]

Received 28th November 2024
Accepted 11th March 2025

DOI: 10.1039/d4ra08430f

rsc.li/rsc-advances

In this work, we prepared a bimetallic–organic framework (bimetallic-MOF) using Fe/Zr as metals. Subsequently, the bimetallic-MOF was functionalized with phosphorus acid groups to serve as a heterogeneous catalyst. The catalyst was characterized using various techniques, such as field emission scanning electron microscopy (FE-SEM), energy-dispersive X-ray spectroscopy (EDS), infrared spectroscopy (FT-IR), X-ray diffraction analysis (XRD) and Brunauer–Emmett–Teller (BET) surface area analysis. Due to its suitable surface area and pore size, this heterogeneous catalyst was used for the preparation of pyrido[2,3-*d*]pyrimidine derivatives, achieving good yields (71–86%). Easy separation of the catalyst from the reaction medium, high yields, short reaction times and catalyst reusability are some of the characteristic advantages of multicomponent reactions.

Introduction

Metal–organic frameworks (MOFs) are an attractive group of nanoporous materials with a crystalline structure, formed by coordinating metal ions with organic ligands. Literature surveys show that MOFs exhibit one-dimensional, two-dimensional and three-dimensional structural topologies.[1,2] The structure, as well as the physical and chemical properties of this compound family, depends on the choice of metals and ligands used.[3–5] Research shows that MOFs, with their outstanding properties such as high surface area and porosity, targeted synthesis capability, high chemical and thermal stability, and well-ordered structures, have vast applications in both laboratory and industrial fields.[6,7] Considering the characteristics of this category of porous compounds, various research groups have explored numerous applications, such as catalysis, photo-catalysis, sensors, capacitors and drug delivery systems.[8–10] The catalytic applications of MOFs have been widely reported, encompassing heterogeneous acid, base, asymmetric, bio- and photo-catalytic systems.[11–13] In recent years, an attractive subclass of MOFs, known as bimetallic–organic frameworks (bimetallic-MOFs), has been introduced. Bimetal-MOFs incorporate two metals into their crystal structure simultaneously, and research findings show that this category of porous materials not only retains the characteristics of single-metal MOFs but also exhibits unique synergistic effects. Bimetallic-MOFs are extensively used in the fabrication of supercapacitors, lithium batteries, and, most notably, as catalysts.[14–16] Among these applications, the catalytic potential of bimetal-MOFs is noteworthy. Consequently, bimetallic-MOFs represent promising candidates for catalyzing organic reactions, such as multicomponent, cross-coupling, click and oxidation–reduction reactions.[17–21] Therefore, we purposefully designed and synthesized UiO-66(Fe/Zr)–NH_2 as a bimetallic catalyst based on iron (Fe) and zirconium (Zr) metals. The introduction of zirconium (Zr) metal enhanced the porosity and increased the number of active sites on the catalyst's surface, while the introduction of iron (Fe) metal greatly improved the catalytic activity and stability of the catalyst. Based on the above information, we designed and synthesized UiO-66(Fe/Zr)–$N(CH_2PO_3H_2)_2$ as a bimetallic-MOF containing Fe and Zr metals to achieve high porosity, abundant active sites, high catalytic strength, and excellent stability. Phosphorous acid derivatives are widely used in various fields as extractors, inhibitors, catalysts, and absorbents. The incorporation of phosphorous acid groups enhances the MOF's ability to accelerate organic reactions effectively. As a result, numerous phosphorous acid-containing catalysts have

[a]*Department of Organic Chemistry, Faculty of Chemistry and Petroleum Sciences, Bu-Ali Sina University, Hamedan 6517838683, Iran. E-mail: zolfi@basu.ac.ir; mzolfigol@yahoo.com; Fax: +988138380709; Tel: +988138282807*

[b]*Department of Chemistry, Faculty of Science, University of Qom, Qom, 37185-359, Iran. E-mail: mahmoud8103@yahoo.com*

[c]*Department of Energy, Materials and Energy Research Center, Karaj 401602, Iran*

† Electronic supplementary information (ESI) available: It includes spectral data of pyrido[2,3-*d*]pyrimidine derivatives. See DOI: https://doi.org/10.1039/d4ra08430f

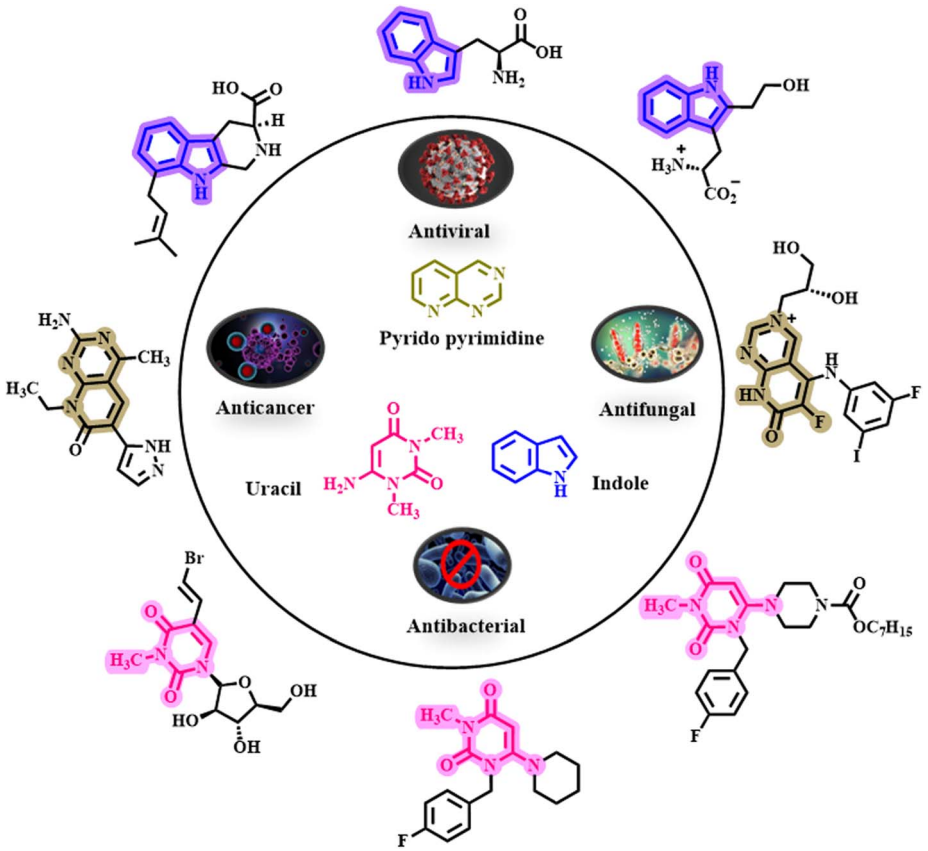

Fig. 1 Structures of medicinal and biological materials based on pyrido pyrimidines, uracil and indole.

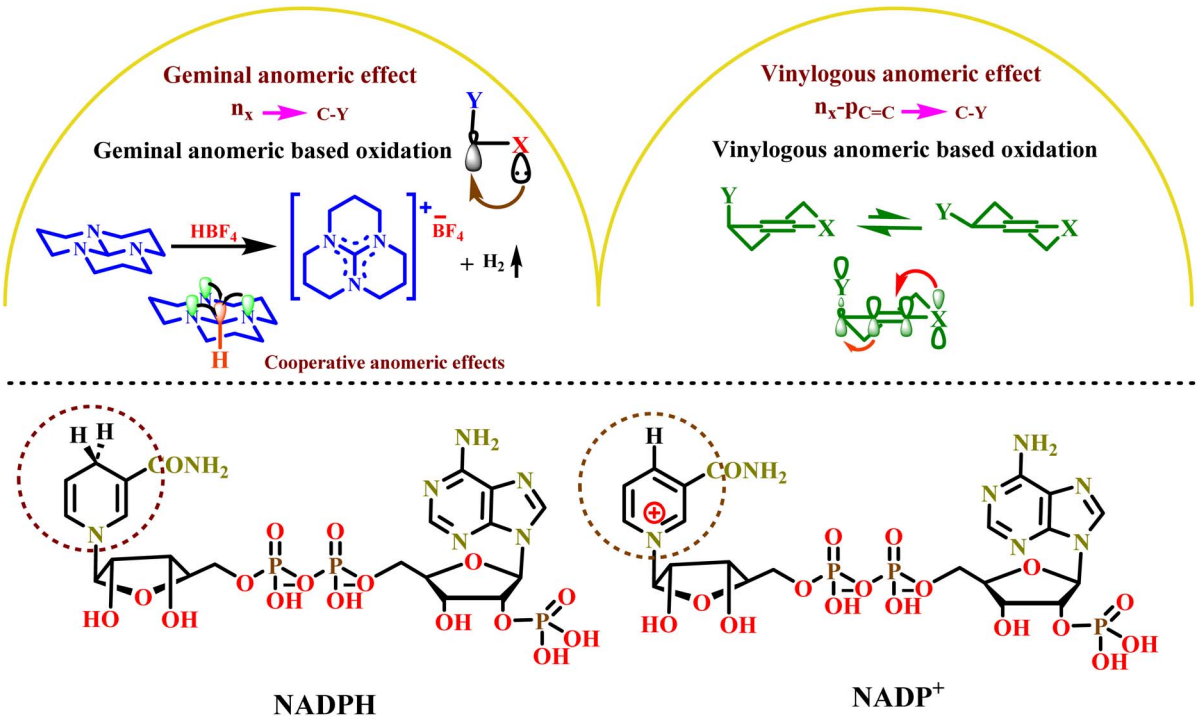

Fig. 2 The geminal and vinylogous anomeric effects on organic and biological compounds.

been synthesized and studied.[22–29] In this study, UiO-66(Fe/Zr)–NH_2 was synthesized as a bimetallic-MOF catalyst and further modified by the introduction of phosphorous acid groups. The concurrent co-existence of iron and zirconium metals created a synergistic effect, while the incorporation of phosphorous acid functional groups resulted in the formation of a new acid catalyst with broad catalytic activity.

In recent years, organic compounds containing indole and uracil skeletons have garnered significant attention due to their biological properties, such as antifungal, anticancer, antibacterial, and antiviral properties. Pyrido[2,3-*d*]pyrimidine derivatives represent a class of organic compounds with diverse medicinal properties, including antitumor, antibacterial, antidepressant, anticonvulsant and antipyretic activities (Fig. 1).[30–32] Considering the medicinal and biological properties of indole, uracil and pyrido[2,3-*d*]pyrimidine compounds, we propose that the target molecules synthesized in this study may also exhibit significant medicinal and biological activities.

The anomeric effect is a subset of stereoelectronic effects involving electron delocalization through space from donor to acceptor atoms.[33,34] Electrons are transferred from a lone pair of heteroatoms (X = N, O, and so on) to the anti-bonding orbital of the C–Y bond ($n_{XN/O} \rightarrow \sigma^*_{C-Y}$), leading to various reported anomeric effects. The anomeric effect, also known as negative hyperconjugation, plays a crucial role in chemical processes, especially in organic reactions.[35,36] The oxidation–reduction possesses of sensitive biological compounds, such as NADPH and $NADP^+$, rely on the anomeric effect, highlighting its significance (Fig. 2). In recent years, our research group has explored the role of the anomeric effect in the *in situ* oxidation of organic compounds without the need for an external oxidant.[37–42] Recently, our study has focused on the anomeric effect, as well as cooperative and vinylogous anomeric-based oxidation (CVABO), which involves electron transfer through a double bond.[33,34]

Experimental section

Materials and methods

6-Amino-1,3-dimethyluracil, indole, 2-methylindole, acetic anhydride, cyanoacetic acid, $ZrCl_4$, $FeCl_3 \cdot 6H_2O$, 2-amino terephthalic acid (NH_2-BDC), *p*-TSA, formaldehyde (HCOH) and various aromatic aldehyde derivatives were purchased from Merck and Sigma-Aldrich. Furthermore, acetic acid (HOAc, 99%), *N*,*N*-dimethylformamide (DMF, 99%), ethanol (EtOH, 99%), methanol (MeOH, 99%), and other solvents were purchased from commercial sources and used without further purification. To analyze the morphology of the final catalyst, scanning electron microscopy (SEM) was performed using a TESCAN MIRA-II (Czechia). In addition, a Fourier transform infrared (FT-IR) spectrometer (PerkinElmer Spectrum Version 10.02.00) was used to determine the functional groups in the catalyst and pure materials. X-ray powder diffraction (XRD) analysis was performed to investigate the crystal structure of the catalyst using PHILIPS PW1730 (Netherlands). Energy-dispersive spectroscopy (EDS) and elemental mapping were carried out using a TESCAN MIRA-II (Czechia). Furthermore, Brunauer–Emmett–Teller (BET) method (BELSORP-mini-II) and the Barrett–Joyner–Halenda (BJH) technique were used to determine the surface area and pore size of the synthesized catalyst. The required starting materials were synthesized according to our recently reported synthetic organic methodology.[43]

Preparation of UiO-66(Fe/Zr)–$N(CH_2PO_3H_2)_2$ as a heterogeneous catalyst

First, UiO-66(Fe/Zr)–NH_2, a bimetallic–organic framework, was synthesized based on previous reports.[44] Then, UiO-66(Fe/Zr)–NH_2 (0.5 g) was dispersed in EtOH (10 mL). In the next step, the activated UiO-66(Fe/Zr)–NH_2 (0.5 g), formaldehyde (4 mmol, 0.12 g), phosphorous acid (2 mmol, 0.164 g), and *p*-TSA (0.01 g) were stirred at room temperature for 12 hours. The resulting precipitate of the bimetallic-MOF functionalized with phosphorous acid groups was centrifuged and washed several times with EtOH. Finally, UiO-66(Fe/Zr)–$N(CH_2PO_3H_2)_2$ was dried at 80 °C for 24 h (Scheme 1).

General procedure for the preparation of pyrido[2,3-*d*] pyrimidines using UiO-66(Fe/Zr)–$N(CH_2PO_3H_2)_2$

First, the starting materials, 3-(1*H*-indol-3-yl)-3-oxopropanenitrile and 3-(2-methyl-1*H*-indol-3-yl)-3-oxopropanenitrile, were synthesized according to previously reported methodologies.[45,46] Then, in a 10 mL round-bottomed flask, a mixture of 3-(1*H*-indol-3-yl)-3-oxopropanenitrile (1 mmol, 0.184 g), aldehyde derivatives (1 mmol) and 6-amino-1,3-dimethylpyrimidine-2,4(1*H*,3*H*)-dione (1 mmol, 0.155 g) was prepared in the presence of UiO-66(Fe/Zr)–$N(CH_2PO_3H_2)_2$ (10 mg) as a novel heterogeneous catalyst. The reaction was carried out at 100 °C under solvent-free conditions. The progress of the reaction was monitored using TLC (EtOAc/*n*-hexane, 1 : 1). Upon completion of the reaction, UiO-66(Fe/Zr)–$N(CH_2PO_3H_2)_2$ was separated from the reaction mixture by centrifugation (1000 rpm) after adding EtOH (10 mL). Finally, the pure product was obtained by washing with cold EtOH (3 × 10 mL) and drying at 100 °C (Scheme 2).

Spectral data of pyrido[2,3-*d*]pyrimidine derivatives

5-(4-Chlorophenyl)-7-(1*H*-indol-3-yl)-1,3-dimethyl-2,4-dioxo-1,2,3,4-tetrahydropyrido[2,3-*d*]pyrimidine-6-carbonitrile (B1).[47] Yellow solid; Mp: > 300°C; FT-IR (KBr, cm^{-1}): 3309, 2223, 1712, 1652, 1554. ^{1}H NMR (400 MHz, DMSO-d_6) δ_{ppm} 12.13 (s, 1H), 8.58 (s, 1H), 8.49–8.42 (m, 1H), 7.57 (d, J = 8.1 Hz, 3H), 7.39 (d, J = 8.1 Hz, 2H), 7.34–7.25 (m, 2H), 3.78 (s, 3H), 3.18 (s, 3H). ^{13}C NMR (101 MHz, DMSO-d_6) δ_{ppm} 160.5, 159.4, 157.5, 152.6, 151.3, 140.1, 136.2, 135.8, 133.9, 130.3, 128.5, 126.9, 122.3, 120.8, 119.8, 117.0, 111.7, 111.0, 105.7, 104.6, 30.4, 28.6.

5-(2-Chlorophenyl)-7-(1*H*-indol-3-yl)-1,3-dimethyl-2,4-dioxo-1,2,3,4-tetrahydropyrido[2,3-*d*]pyrimidine-6-carbonitrile (B2). Yellow solid; Mp: > 300°C; FT-IR (KBr, cm^{-1}): 3256, 2221, 1722, 1655, 1557. ^{1}H NMR (400 MHz, DMSO-d_6) δ_{ppm} 12.17 (s, 1H), 8.60 (s, 1H), 7.63 (d, J = 8.1 Hz, 2H), 7.54–7.48 (m, 2H), 7.38 (d, J = 7.4 Hz, 1H), 7.35–7.22 (m, 3H), 3.81 (s, 3H), 3.19 (s, 3H). ^{13}C NMR (101 MHz, DMSO-d_6) δ_{ppm} 159.3, 158.9, 156.0, 153.0,

151.2, 136.6, 132.2, 131.7, 130.7, 129.6, 129.5, 127.8, 127.7, 126.2, 124.1, 123.6, 123.1, 122.3, 122.2, 121.7, 119.0, 113.0, 30.9, 28.6. MS *m*/*z* (%) found for $C_{24}H_{16}ClN_5O_2$: 441.1.

5-(4-Bromophenyl)-7-(1*H*-indol-3-yl)-1,3-dimethyl-2,4-dioxo-1,2,3,4-tetrahydropyrido[2,3-*d*]pyrimidine-6-carbonitrile (B3).[47] Yellow solid; Mp: > 300°C; FT-IR (KBr, cm^{-1}): 3342, 2213, 1708, 1657, 1517. ^{1}H NMR (400 MHz, DMSO-d_6) δ_{ppm} 12.14 (s, 1H), 8.58 (s, 1H), 8.46 (s, 1H), 7.71 (d, J = 8.0 Hz, 2H), 7.59 (s, 1H), 7.40–7.23 (m, 4H), 3.79 (s, 3H), 3.18 (s, 3H). ^{13}C NMR (101 MHz, DMSO-d_6) δ_{ppm} 158.7, 158.5, 157.2, 152.4, 150.7, 136.5, 136.3, 131.2, 130.9, 129.8, 125.7, 123.0, 121.9, 121.7, 121.6, 117.7, 112.5, 112.1, 104.2, 100.1, 30.4, 28.1.

7-(1*H*-indol-3-yl)-1,3-dimethyl-2,4-dioxo-5-phenyl-1,2,3,4-tetrahydropyrido[2,3-*d*]pyrimidine-6-carbonitrile (B4).[47] Yellow solid; Mp: > 300°C; FT-IR (KBr, cm^{-1}): 3322, 2212, 1704, 1655, 1548. ^{1}H NMR (400 MHz, DMSO-d_6) δ_{ppm} 12.12 (s, 1H), 8.57 (s, 1H), 8.48–8.44 (m, 1H), 7.60–7.55 (m, 1H), 7.51–7.47 (m, 3H), 7.34 (dd, J = 6.6, 2.9 Hz, 2H), 7.31–7.27 (m, 2H), 3.78 (s, 3H), 3.17 (s, 3H). ^{13}C NMR (101 MHz, DMSO-d_6) δ_{ppm} 158.5, 158.3, 152.3, 150.7, 136.9, 136.5, 131.1, 128.3, 127.8, 127.4, 125.7, 122.9, 121.7, 121.6, 117.7, 112.4, 112.1, 104.1, 100.3, 30.4, 28.0.

5-(3-Hydroxyphenyl)-7-(1*H*-indol-3-yl)-1,3-dimethyl-2,4-dioxo-1,2,3,4tetrahydropyrido[2,3-*d*]pyrimidine-6-carbonitrile (B5). Yellow solid; Mp: > 300°C; FT-IR (KBr, cm^{-1}): 3457, 2219, 1705, 1652, 1556. ^{1}H NMR (400 MHz, DMSO-d_6) δ_{ppm} 12.11 (s, 1H), 9.57 (s, 1H), 8.57 (s, 1H), 8.48–8.42 (m, 1H), 7.60–7.55 (m, 1H), 7.32–7.24 (m, 3H), 6.86 (dd, J = 8.2, 1.4 Hz, 1H), 6.76–6.67 (m, 2H), 3.77 (s, 3H), 3.18 (s, 3H). ^{13}C NMR (101 MHz, DMSO-d_6) δ_{ppm} 162.3, 158.6, 158.3, 156.8, 152.4, 150.8, 138.2, 136.5, 131.1, 129.1, 125.8, 122.9, 121.6, 118.0, 117.7, 115.3, 114.3, 112.4, 112.1, 104.3, 100.3, 30.4, 28.0. MS *m*/*z* (%) found for $C_{24}H_{17}N_5O_3$: 423.1.

5-(4-Hydroxyphenyl)-7-(1*H*-indol-3-yl)-1,3-dimethyl-2,4-dioxo-1,2,3,4tetrahydropyrido[2,3-*d*]pyrimidine-6-carbonitrile (B6). Yellow solid; Mp: > 300°C; FT-IR (KBr, cm^{-1}): 3341, 2216, 1696, 1646, 1545. ^{1}H NMR (400 MHz, DMSO-d_6) δ_{ppm} 12.09 (s, 1H), 9.71 (s, 1H), 8.49 (d, J = 50.0 Hz, 2H), 7.56 (s, 1H), 7.33–7.10 (m, 4H), 6.85 (s, 2H), 3.73 (s, 3H), 3.17 (s, 3H). ^{13}C NMR (101 MHz, DMSO-d_6) δ_{ppm} 159.5, 159.1, 158.9, 158.3, 152.9, 151.3, 137.0, 131.6, 129.8, 128.4, 126.3, 123.4, 122.1, 122.1, 115.2, 112.9, 112.7, 104.9, 101.3, 30.9, 28.6.

7-(1*H*-indol-3-yl)-5-(4-methoxyphenyl)-1,3-dimethyl-2,4-dioxo-1,2,3,4-tetrahydropyrido[2,3-*d*]pyrimidine-6-carbonitrile (B7).[47] Yellow solid; Mp: > 300°C; FT-IR (KBr, cm^{-1}): 3434, 2218, 1713, 1661, 1516. ^{1}H NMR (400 MHz, DMSO-d_6) δ_{ppm} 12.10 (s, 1H), 8.57 (d, J = 2.9 Hz, 1H), 8.46–8.43 (m, 1H), 7.59–7.56 (m, 1H), 7.30–7.27 (m, 4H), 7.04 (d, J = 8.7 Hz, 2H), 3.86 (s, 3H), 3.77 (s, 3H), 3.18 (s, 3H). ^{13}C NMR (101 MHz, DMSO-d_6) δ_{ppm} 159.4, 158.6, 158.5, 158.4, 152.5, 150.8, 136.5, 131.1, 129.2, 128.9, 125.8, 122.9, 121.6, 118.0, 113.2, 112.4, 112.2, 104.5, 100.8, 55.1, 30.4, 28.1.

7-(1*H*-indol-3-yl)-1,3-dimethyl-2,4-dioxo-5-(*m*-tolyl)-1,2,3,4-tetrahydropyrido[2,3-*d*]pyrimidine-6-carbonitrile (B8). Yellow solid; Mp: > 300°C; FT-IR (KBr, cm^{-1}): 3479, 2216, 1712, 1662, 1550. ^{1}H NMR (400 MHz, DMSO-d_6) δ_{ppm} 12.11 (s, 1H), 8.57 (s, 1H), 8.46 (dd, J = 6.5, 2.7 Hz, 1H), 7.61–7.56 (m, 1H), 7.38 (t, J = 7.6 Hz, 1H), 7.32–7.27 (m, 3H), 7.16–7.11 (m, 2H), 3.79 (s, 3H), 3.18 (s, 3H), 2.39 (s, 3H). ^{13}C NMR (101 MHz, DMSO-d_6) δ_{ppm} 160.5, 159.4, 157.5, 152.6, 151.3, 140.1, 136.2, 135.8, 133.9, 130.3, 128.5, 126.9, 122.3, 120.8, 119.8, 117.0, 111.7, 111.0, 105.7, 104.6, 30.4, 28.6, 14.3. MS *m*/*z* (%) found for $C_{25}H_{19}N_5O_2$: 421.1.

7-(1*H*-indol-3-yl)-1,3-dimethyl-2,4-dioxo-5-(*p*-tolyl)-1,2,3,4-tetrahydropyrido[2,3-*d*]pyrimidine-6-carbonitrile (B9).[47] Yellow solid; Mp: > 300°C; FT-IR (KBr, cm^{-1}): 3313, 2223, 1710, 1650, 1554. ^{1}H NMR (500 MHz, DMSO) δ_{ppm} 12.06 (s, 1H), 8.53 (s, 1H), 8.40 (d, J = 7.9 Hz, 1H), 7.53 (d, J = 8.1 Hz, 1H), 7.30–7.21 (m, 4H), 7.16 (d, J = 8.6 Hz, 2H), 3.67 (s, 3H), 3.12 (s, 3H), 2.41 (s, 3H). ^{13}C NMR (126 MHz, DMSO-d_6) δ_{ppm} 158.7, 158.4, 158.3, 152.3, 150.6, 137.7, 136.5, 134.0, 131.1, 128.4, 127.5, 125.8, 122.9, 121.7, 121.6, 117.9, 112.4, 112.2, 104.1, 100.3, 30.4, 28.0, 21.0.

5,7-Di(1*H*-indol-3-yl)-1,3-dimethyl-2,4-dioxo-1,2,3,4-tetrahydropyrido[2,3-*d*]pyrimidine-6-carbonitrile (B10). Yellow solid; Mp: > 300°C; FT-IR (KBr, cm^{-1}): 3432, 2210, 1702, 1653, 1543. ^{1}H NMR (400 MHz, DMSO-d_6) δ_{ppm} 11.85 (s, 1H), 11.33 (s, 1H), 8.31 (s, 1H), 8.23–8.18 (m, 1H), 7.46 (d, J = 2.6 Hz, 1H), 7.34–7.30 (m, 1H), 7.25 (d, J = 8.1 Hz, 1H), 7.04 (t, J = 7.6 Hz, 3H), 6.91 (t, J = 7.6 Hz, 1H), 6.76 (t, J = 7.5 Hz, 1H), 3.52 (s, 3H), 2.90 (s, 3H). ^{13}C NMR (101 MHz, DMSO-d_6) δ_{ppm} 158.9, 158.5, 152.8, 152.2, 150.9, 136.5, 135.9, 131.1, 126.5, 126.4, 125.8, 122.8, 121.6, 121.5, 121.4, 119.5, 119.3, 119.0, 112.4, 112.3, 111.8, 110.9, 105.0, 101.3, 30.4, 28.1.

5-(4-Chlorophenyl)-1,3-dimethyl-7-(2-methyl-1*H*-indol-3-yl)-2,4-dioxo-1,2,3,4-tetrahydropyrido[2,3-*d*]pyrimidine-6-carbonitrile (C1).[48] Yellow solid; Mp: > 300°C; FT-IR (KBr, cm^{-1}): 3309, 2223, 1712, 1652, 1554. ^{1}H NMR (400 MHz, DMSO-d_6) δ_{ppm} 11.90 (s, 1H), 7.75 (d, J = 7.3 Hz, 1H), 7.58 (d, J = 8.5 Hz, 2H), 7.48 (d, J = 8.4 Hz, 2H), 7.43 (d, J = 7.2 Hz, 1H), 7.20–7.11 (m, 2H), 3.67 (s, 3H), 3.20 (s, 3H), 2.62 (s, 3H). ^{13}C NMR (101 MHz, DMSO-d_6) δ_{ppm} 160.5, 159.4, 157.5, 152.6, 151.3, 140.1, 136.2, 135.8, 133.9, 130.3, 128.5, 126.9, 122.3, 120.8, 119.8, 117.0, 111.7, 111.0, 105.7, 104.6, 30.4, 28.6, 14.3.

5-(4-Hydroxyphenyl)-1,3-dimethyl-7-(2-methyl-1*H*-indol-3-yl)-2,4-dioxo-1,2,3,4-tetrahydropyrido[2,3-*d*]pyrimidine-6-carbonitrile (C2). Yellow solid; Mp: > 300°C; FT-IR (KBr, cm^{-1}): 3454, 3314, 2213, 1712, 1651. ^{1}H NMR (400 MHz, DMSO-d_6) δ_{ppm} 11.62 (s, 1H), 9.52 (s, 1H), 7.50 (d, J = 7.2 Hz, 1H), 7.17 (d, J = 7.1 Hz, 1H), 7.00 (d, J = 8.6 Hz, 2H), 6.93–6.88 (m, 2H), 6.62 (d, J = 8.6 Hz, 2H), 3.40 (s, 3H), 2.95 (s, 3H), 2.37 (s, 3H). ^{13}C NMR (101 MHz, DMSO-d_6) δ_{ppm} 159.9, 158.9, 158.6, 158.0, 152.2, 150.8, 139.4, 135.2, 129.7, 126.9, 126.5, 121.7, 120.3, 119.3, 117.0, 115.2, 114.7, 111.2, 110.6, 105.1, 104.6, 29.9, 28.1, 13.9. MS *m*/*z* (%) found for $C_{25}H_{19}N_5O_3$: 437.1.

5-(4-Methoxyphenyl)-1,3-dimethyl-7-(2-methyl-1*H*-indol-3-yl)-2,4-dioxo-1,2,3,4-tetrahydropyrido[2,3-*d*]pyrimidine-6-carbonitrile (C3). Yellow solid; Mp: > 300°C; FT-IR (KBr, cm^{-1}): 3311, 2223, 1713, 1651, 1533. ^{1}H NMR (400 MHz, DMSO-d_6) δ_{ppm} 11.64 (s, 1H), 7.51 (d, J = 7.6 Hz, 1H), 7.18 (d, J = 7.7 Hz, 1H), 7.13 (d, J = 8.3 Hz, 2H), 6.95–6.87 (m, 2H), 6.81 (d, J = 8.3 Hz, 2H), 3.61 (s, 3H), 3.41 (s, 3H), 2.95 (s, 3H), 2.38 (s, 3H). ^{13}C NMR (101 MHz, DMSO-d_6) δ_{ppm} 159.9, 159.6, 158.9, 158.2, 152.2, 150.8, 139.5, 135.2, 129.6, 128.6, 126.4, 121.8, 120.3,

119.3, 116.9, 113.3, 111.2, 110.6, 105.2, 104.5, 55.1, 29.9, 28.1, 13.8. MS *m*/*z* (%) found for $C_{26}H_{21}N_5O_3$: 451.2.

1,3-Dimethyl-7-(2-methyl-1*H*-indol-3-yl)-2,4-dioxo-5-(*p*-tolyl)-1,2,3,4-tetrahydropyrido[2,3-*d*]pyrimidine-6-carbonitrile (C4). Yellow solid; Mp: > 300°C; FT-IR (KBr, cm^{-1}): 3313, 2223, 1710, 1650, 1554. ^{1}H NMR (400 MHz, DMSO-d_6) δ_{ppm} 11.64 (s, 1H), 7.50 (d, J = 7.2 Hz, 1H), 7.18 (d, J = 7.3 Hz, 1H), 7.08–7.03 (m, 4H), 6.94–6.87 (m, 2H), 3.41 (s, 3H), 2.94 (s, 3H), 2.37 (s, 3H), 2.17 (s, 3H). ^{13}C NMR (101 MHz, DMSO-d_6) δ_{ppm} 160.0, 158.8, 158.4, 152.2, 150.8, 139.5, 137.9, 135.2, 133.8, 128.5, 127.8, 126.4, 121.7, 120.3, 119.3, 116.8, 111.2, 110.6, 105.1, 104.4, 29.9, 28.1, 21.0, 13.9. MS *m*/*z* (%) found for $C_{26}H_{21}N_5O_2$: 435.2.

5-(2-Chlorophenyl)-7-(1*H*-indol-3-yl)-1,3-dimethyl-2,4-dioxo-1,2,3,4-tetrahydropyrido[2,3-*d*]pyrimidine-6-carbonitrile (C5). Yellow solid; Mp: > 300°C; FT-IR (KBr, cm^{-1}): 3355, 2245, 1720, 1673, 1557. ^{1}H NMR (400 MHz, DMSO-d_6) δ_{ppm} 11.72 (s, 1H), 7.47 (dd, J = 7.3, 1.5 Hz, 1H), 7.39 (dd, J = 7.6, 1.7 Hz, 1H), 7.30–7.23 (m, 2H), 7.20–7.17 (m, 2H), 6.91 (ddd, J = 9.2, 7.5, 1.4 Hz, 2H), 3.43 (s, 3H), 2.95 (s, 3H), 2.36 (s, 3H). ^{13}C NMR (101 MHz, DMSO-d_6) δ_{ppm} 160.2, 158.6, 155.0, 152.2, 150.7, 139.6, 135.9, 135.3, 130.5, 130.3, 129.2, 129.0, 127.2, 126.3, 121.9, 120.4, 119.1, 116.0, 111.3, 110.4, 105.3, 103.9, 29.9, 28.1, 13.8. MS *m*/*z* (%) found for $C_{25}H_{18}ClN_5O_2$: 455.1.

5-(3,4-Dimethoxyphenyl)-1,3-dimethyl-7-(2-methyl-1*H*-indol-3-yl)-2,4-dioxo-1,2,3,4-tetrahydropyrido[2,3-*d*]pyrimidine-6-carbonitrile (C6). Yellow solid; Mp: > 300°C; FT-IR (KBr, cm^{-1}): 3358, 2223, 1718, 1676, 1543. ^{1}H NMR (400 MHz, DMSO-d_6) δ_{ppm} 11.66 (s, 1H), 7.51 (d, J = 8.7 Hz, 1H), 7.18 (d, J = 7.0 Hz, 1H), 6.95–6.88 (m, 2H), 6.83 (d, J = 8.3 Hz, 1H), 6.79 (d, J = 2.0 Hz, 1H), 6.74 (dd, J = 8.2, 2.0 Hz, 1H), 3.60 (s, 3H), 3.50 (s,

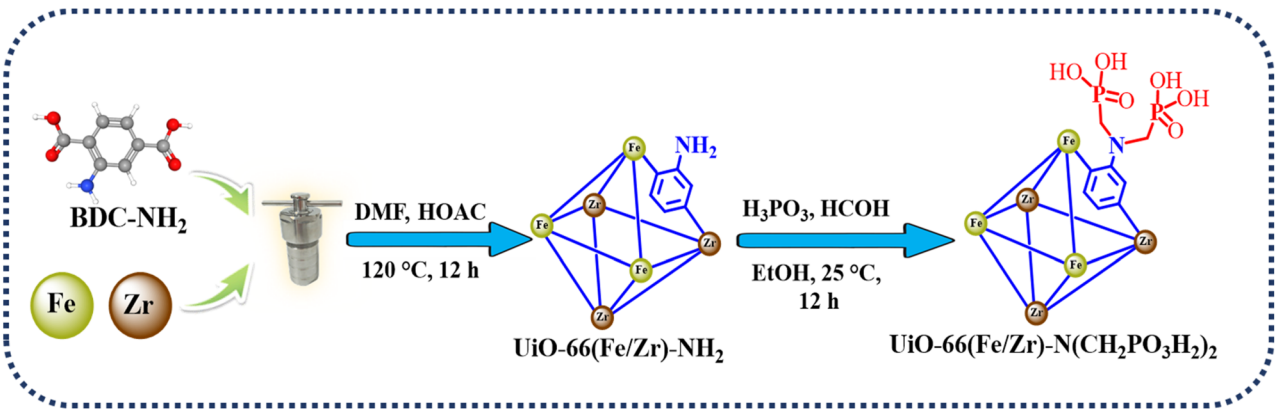

Scheme 1 Schematic strategy for the preparation of UiO-66(Fe/Zr)–$N(CH_2PO_3H_2)_2$.

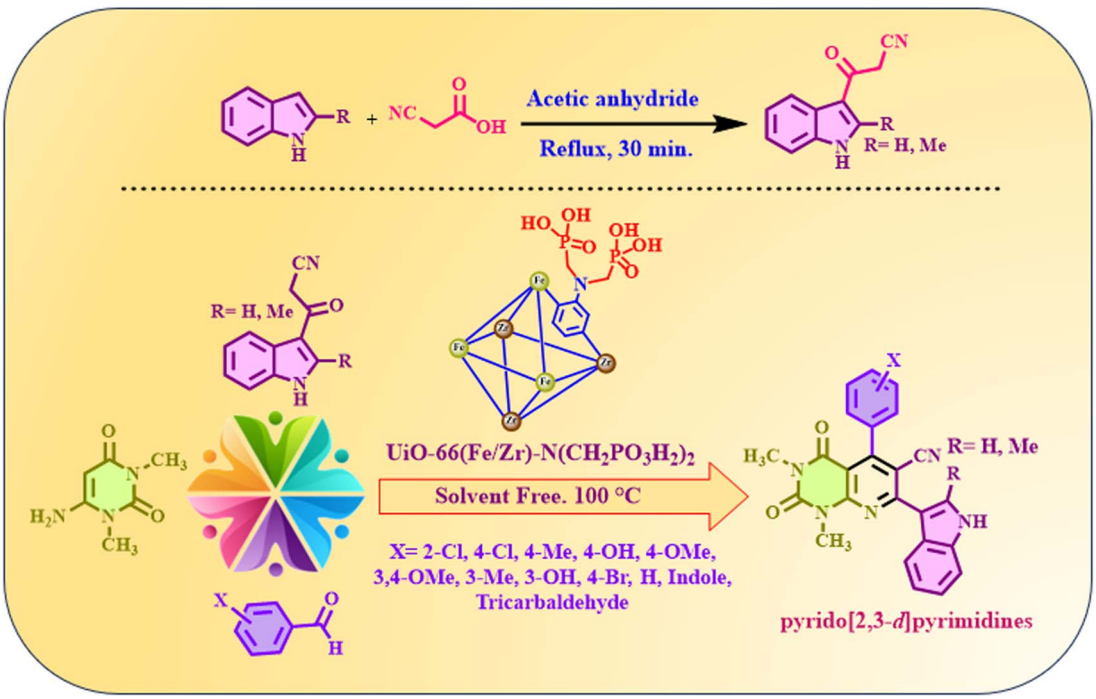

Scheme 2 Synthesis of pyrido[2,3-*d*]pyrimidines using UiO-66(Fe/Zr)–$N(CH_2PO_3H_2)_2$.

3H), 3.42 (s, 3H), 2.96 (s, 3H), 2.38 (s, 3H). ^{13}C NMR (101 MHz, DMSO-d_6) δ_{ppm} 159.9, 158.8, 158.2, 152.1, 150.8, 149.1, 148.0, 139.5, 135.2, 128.9, 126.5, 121.8, 120.7, 120.3, 119.3, 116.9, 112.2, 111.2, 111.0, 110.6, 105.3, 104.6, 55.6, 55.4, 29.9, 28.1, 13.8.

5,5′,5″–(((1,3,5-Triazine-2,4,6-triyl)tris(oxy))tris(benzene-4,1-diyl))tris(7-(1*H*-indol-3-yl)-1,3-dimethyl-2,4-dioxo-1,2,3,4-tetrahydropyrido[2,3-*d*]pyrimidine-6-carbonitrile) (C7). Yellow solid; Mp: > 300°C; FT-IR (KBr, cm^{-1}): 3343, 2219, 1696, 1646, 1554. ^{1}H NMR (400 MHz, DMSO-d_6) δ_{ppm} 11.87 (s, 3H), 9.48 (s, 3H), 8.31 (s, 2H), 8.21–8.18 (m, 3H), 7.33–7.31 (m, 2H), 7.11 (d, J = 8.5 Hz, 2H), 7.05–7.03 (m, 4H), 6.92 (d, 4H), 6.60 (d, J = 8.6 Hz, 4H), 3.54 (s, 9H), 3.52 (s, 9H), 2.93 (s, 9H). ^{13}C NMR (101 MHz, DMSO-d_6) δ_{ppm} 165.2, 162.7, 159.0, 158.7, 158.4, 158.2, 157.7, 152.5, 150.8, 136.5, 133.5, 131.1, 128.5, 127.2, 125.8, 122.9, 121.6, 118.1, 114.7, 112.4, 112.2, 104.5, 100.9, 30.4, 28.1.

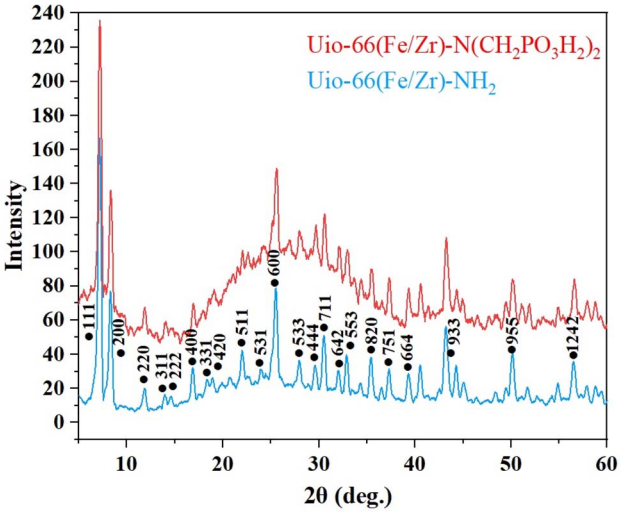

Fig. 4 XRD patterns of UiO-66(Fe/Zr)–NH_2 and UiO-66(Fe/Zr)–$N(CH_2PO_3H_2)_2$.

Results and discussion

In continuation of our investigation based on the principles of green chemistry, we aimed to develop catalytic systems consisting of bimetallic MOFs functionalized with phosphorous acid groups as novel and efficient catalysts. To achieve this, UiO-66(Fe/Zr)–$N(CH_2PO_3H_2)_2$ was synthesized, characterized and applied in the target synthetic method (Scheme 2). Various techniques, such as FT-IR, XRD, BET/BJH and SEM, were utilized for its characterization. Subsequently, this porous catalyst was employed in the preparation of pyrido[2,3-*d*]pyrimidine derivatives as potential biological candidates. Pyrido[2,3-*d*]pyrimidines were prepared using multi-component reactions in the presence of catalytic amounts of the described catalyst (Scheme 2). The mechanism and stereochemistry of the above-mentioned compounds were also investigated. Mechanistic studies revealed that all derivatives

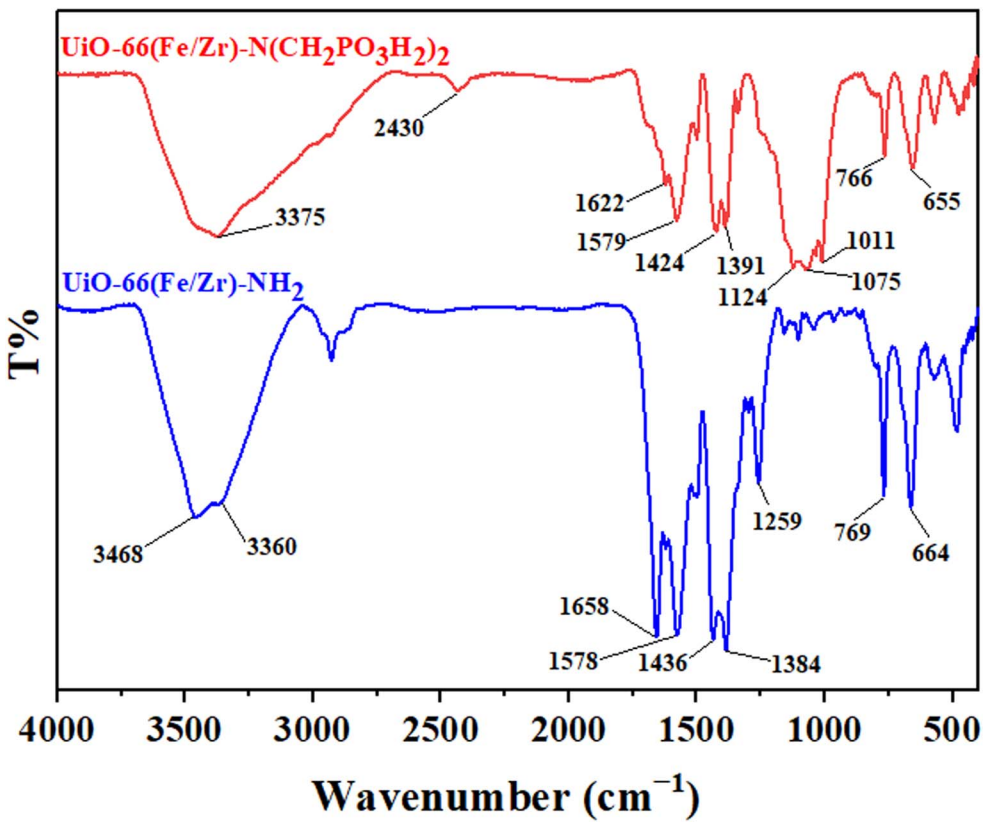

Fig. 3 FT-IR spectra of UiO-66(Fe/Zr)–NH_2 and UiO-66(Fe/Zr)–$N(CH_2PO_3H_2)_2$.

were synthesized using the UiO-66(Fe/Zr)–$N(CH_2PO_3H_2)_2$ catalyst *via* a cooperative vinylogous anomeric-based oxidation mechanism. Finally, the structures of the pyrido[2,3-*d*]pyrimidine derivatives were confirmed using FT-IR, ^{1}H-NMR and ^{13}C-NMR techniques.

To investigate the functional groups present in the catalyst structure, FT-IR analysis was performed. For this purpose, the FT-IR spectra of UiO-66(Fe/Zr)–NH_2 and UiO-66(Fe/Zr)–$N(CH_2PO_3H_2)_2$ were compared (Fig. 3). The broad peak at 2650–3500 cm^{-1} corresponded to the O–H stretching vibration of the

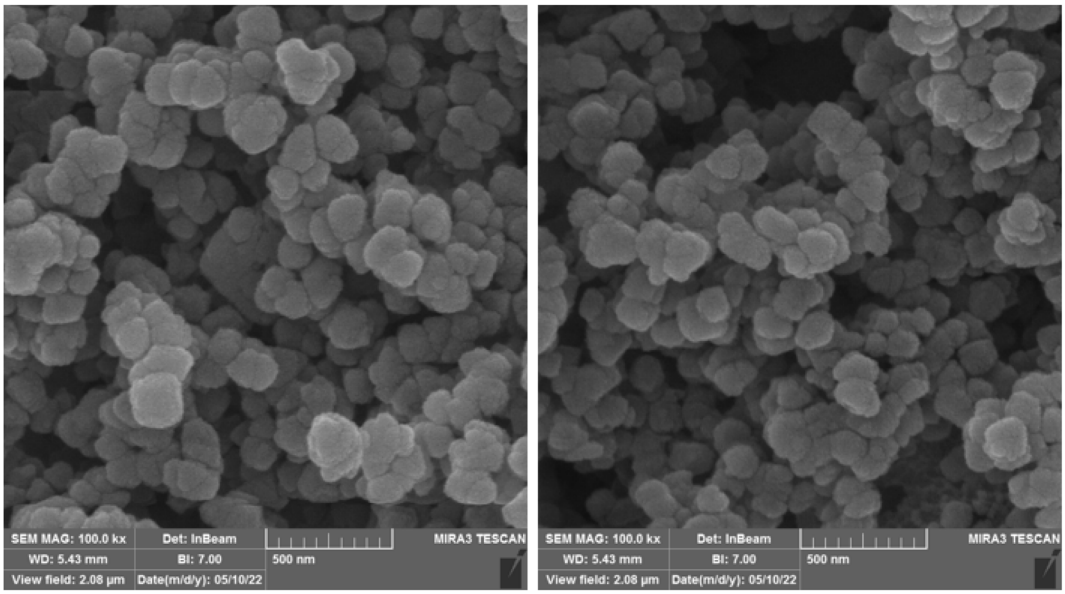

Fig. 5 Scanning electron microscopy (SEM) images of UiO-66(Fe/Zr)–$N(CH_2PO_3H_2)_2$.

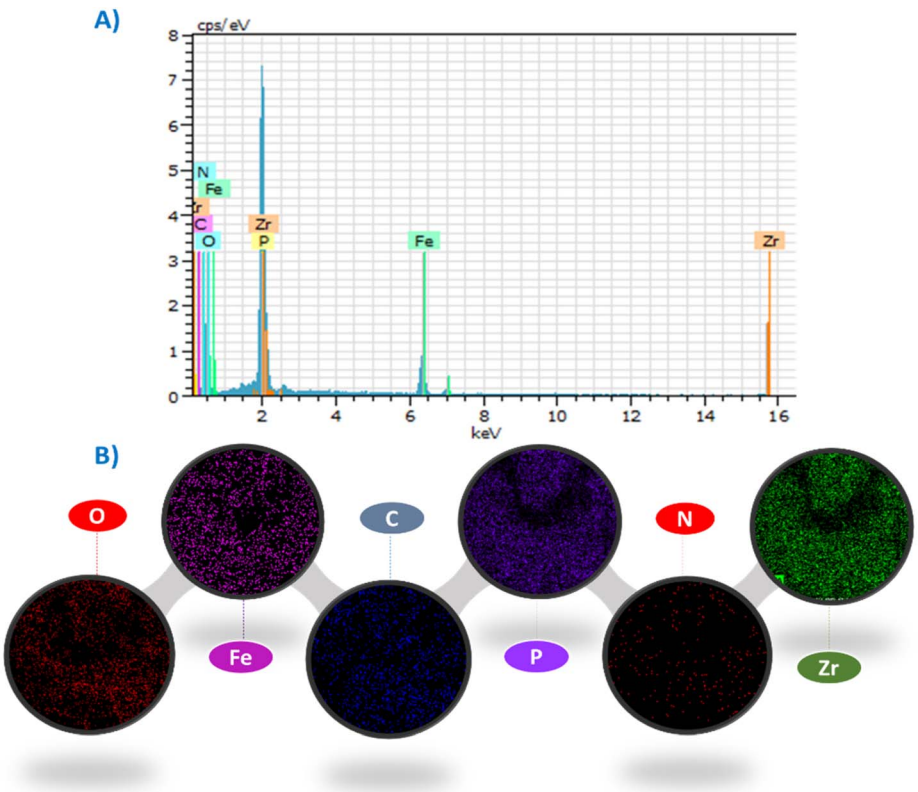

Fig. 6 (A) Energy dispersive X-ray analysis (EDX) and (B) SEM-elemental mapping analysis of UiO-66(Fe/Zr)–$N(CH_2PO_3H_2)_2$.

phosphorous acid group. The absorption peak from 1011 cm^{-1} to 1124 cm^{-1} is related to the P–O and PO stretching vibrations. The differences in the absorption bands between UiO-66(Fe/Zr)–NH_2 and UiO-66(Fe/Zr)–$N(CH_2PO_3H_2)_2$ confirmed the successful incorporation of phosphorous acid groups into the primary bimetallic MOF.

In another investigation, a comparison of UiO-66(Fe/Zr)–NH_2 and UiO-66(Fe/Zr)–$N(CH_2PO_3H_2)_2$ crystal patterns was conducted using XRD analysis (Fig. 4). The crystal pattern of UiO-66(Fe/Zr)–NH_2 was in accordance with a previous report.[44] Examination of the XRD pattern of UiO-66(Fe/Zr)–$N(CH_2PO_3H_2)_2$ revealed that the crystal pattern remained intact even after the incorporation of phosphorous acid groups into the primary catalyst. The appearance of new peaks in the XRD pattern indicated the successful incorporation of phosphorous acid groups. This investigation confirmed the successful formation of bimetallic MOF functionalized with phosphorus acid while preserving its crystal structure.

Scanning electron microscopy (SEM) was utilized to determine the particle size and morphology. As shown in Fig. 5, phosphorous acid groups were successfully incorporated into the original catalyst. During the final synthesis step, the attachment of the phosphorous acid groups to UiO-66(Fe/Zn)–NH_2 did not affect its morphology, indicating that the catalyst structure remained intact.

To study the structure of the catalyst, energy-dispersive X-ray spectroscopy (EDX) and SEM elemental mapping analysis were performed. The presence of carbon (C), oxygen (O), iron (Fe), nitrogen (N), zirconium (Zr) and phosphorus (P) was confirmed (Fig. 6a). Also, SEM elemental mapping analysis (Fig. 6b) clearly demonstrated the uniform distribution of these elements.

The textural properties of UiO-66(Fe/Zr)–$N(CH_2PO_3H_2)_2$ were studied using N_2 adsorption–desorption isotherm analysis (Fig. 7a). Based on the results obtained from BET analysis, the specific surface area of UiO-66(Fe/Zr)–$N(CH_2PO_3H_2)_2$ was 173 $m^2\ g^{-1}$. Also, the total pore volume of the functionalized bimetallic MOF with phosphorous acid groups was 0.262 cm^3g^{-1}. The BJH diagram of UiO-66(Fe/Zr)–$N(CH_2PO_3H_2)_2$ is shown in Fig. 7b. Based on the obtained results, the pore size distribution of UiO-66(Fe/Zr)–$N(CH_2PO_3H_2)_2$ was found to be 6.04 nm.

Table 1 Optimization of some reaction parameters using UiO-66(Fe/Zr)–$N(CH_2PO_3H_2)_2$ as the new porous bimetallic catalyst

Entry	Solvent	Catalyst (mg)	Temp. (°C)	Time (min)	Yield (%)
1	—	—	100	120	—
2	—	5	100	40	60
3	—	7	100	25	73
4	—	10	100	15	85
5	—	15	100	15	85
6	MeOH	10	Reflux	75	25
7	EtOH	10	Reflux	60	35
8	H_2O	10	Reflux	180	—
9	EtOAc	10	Reflux	45	15
10	CH_2Cl_2	10	Reflux	240	—
11	Acetone	10	Reflux	90	20
12	$CHCl_3$	10	Reflux	120	—
13	*n*-Hexane	10	Reflux	120	—
14	—	10	25	120	—
15	—	10	50	70	27
16	—	10	75	60	55
17	—	10	110	15	83

Catalytic activity

After the synthesis and characterization of UiO-66(Fe/Zr)–$N(CH_2PO_3H_2)_2$, the catalyst was employed in the synthesis of pyrido[2,3-*d*]pyrimidine derivatives through the reaction of 6-amino-1,3-dimethylpyrimidine-2,4(1*H*,3*H*)-dione (1 mmol, 0.155 g), 3-(1*H*-indol-3-yl)-3-oxopropanenitrile (1 mmol, 0.184 g), and 4-chlorobenzaldehyde (1 mmol, 0.14 g) as a model reaction. To investigate the optimal reaction conditions, the model reaction was studied in various solvents, such as *n*-hexane, EtOAc, H_2O, MeOH, acetone, $CHCl_3$, CH_2Cl_2, EtOH and under solvent-free conditions. Additionally, the model reaction was performed at different temperatures and catalyst amounts to determine the optimal conditions. Based on the data presented in Table 1, it can be observed that the optimal conditions for the preparation of pyrido[2,3-*d*]pyrimidines were achieved

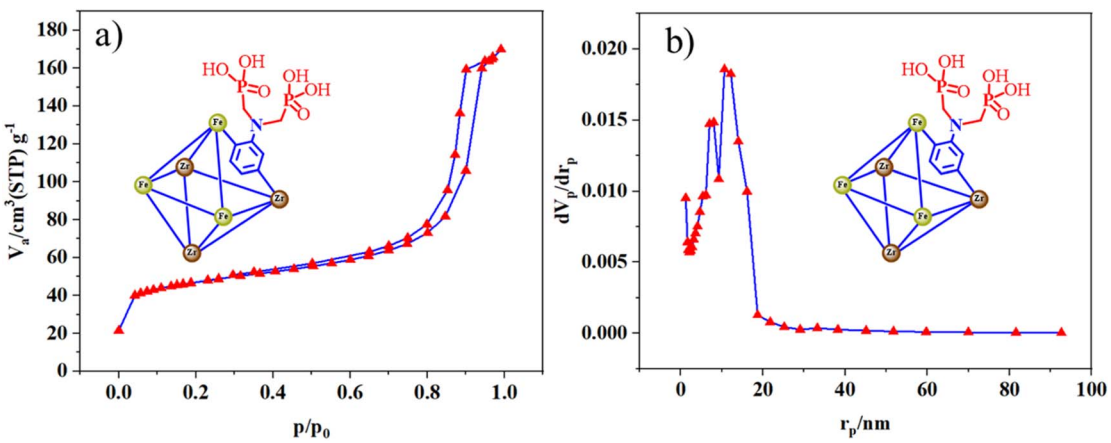

Fig. 7 (a) N_2 adsorption–desorption isotherm and (b) BJH of UiO-66(Fe/Zr)–$N(CH_2PO_3H_2)_2$ as the new porous bimetallic catalyst.

Table 2 Applicability and efficiency of UiO-66(Fe/Zr)–$N(CH_2PO_3H_2)_2$ in the synthesis of pyrido[2,3-*d*]pyrimidine derivatives under solvent-free conditions

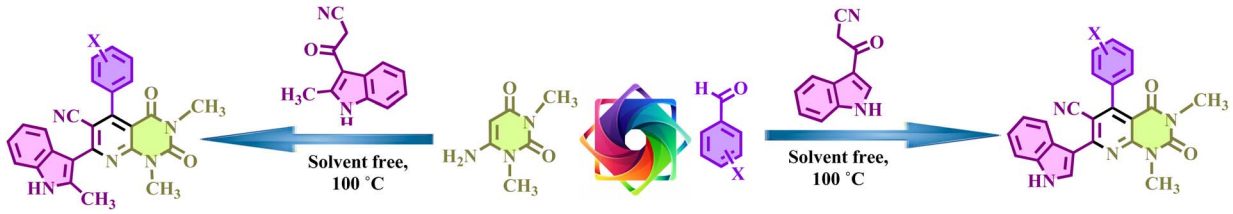

B1
M.p (°C): >300[47]
Time (min.): 15
Yield (%): 85

B2
M.p (°C): >300
Time (min.): 16
Yield (%): 79

B3
M.p (°C): >300[47]
Time (min.):17
Yield (%): 84

B4
M.p (°C): >300[47]
Time (min.): 16
Yield (%): 80

B5
M.p (°C): >300
Time (min.): 18
Yield (%): 75

B6
M.p (°C): >300
Time (min.): 16
Yield (%): 77

B7
M.p (°C): >300[47]
Time (min.): 15
Yield (%): 84

B8
M.p (°C): >300
Time (min.): 16
Yield (%): 78

B9
M.p (°C): >300[47]
Time (min.): 15
Yield (%): 82

B10
M.p (°C): >300
Time (min.): 18
Yield (%): 86

C1
M.p (°C): >300[48]
Time (min.): 17
Yield (%): 84

C2
M.p (°C): >300
Time (min.): 16
Yield (%): 77

C3
M.p (°C): >300
Time (min.): 15
Yield (%): 79

C4
M.p (°C): >300
Time (min.): 15
Yield (%): 82

C5
M.p (°C): >300
Time (min.): 17
Yield (%): 71

C6
M.p (°C): >300
Time (min.): 16
Yield (%): 83

C7
M.p (°C): >300
Time (min.): 15
Yield (%): 82

using UiO-66(Fe/Zr)–$N(CH_2PO_3H_2)_2$ (10 mg) under solvent-free condition at 100 °C.

After the optimal conditions were obtained for the synthesis of pyrido[2,3-*d*]pyrimidine derivatives, the efficiency and applicability of UiO-66(Fe/Zr)–$N(CH_2PO_3H_2)_2$ were studied for various aromatic aldehydes, including those with electron-withdrawing, electron-releasing and heterocyclic groups. The results are shown in Table 2. According to Table 2, the desired

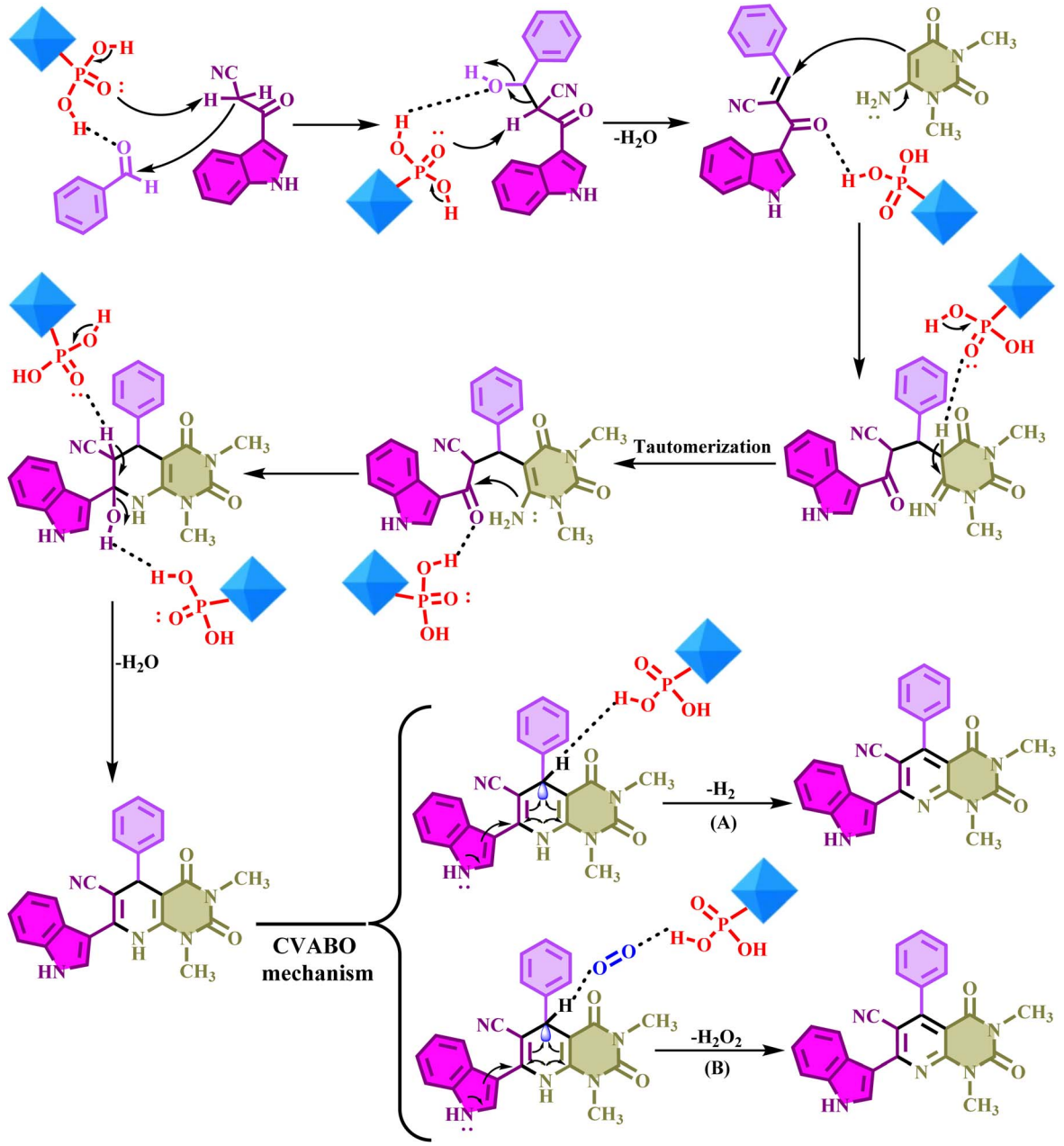

Scheme 3 Proposed mechanism for the synthesis of pyrido[2,3-*d*]pyrimidines using UiO-66(Fe/Zr)–$N(CH_2PO_3H_2)_2$.

products were successfully synthesized with high yields and short reaction times under green and mild conditions.

In the proposed mechanism, the aldehyde is activated by the OH group of PO_3H_2 on UiO-66(Fe/Zr)–$N(CH_2PO_3H_2)_2$. Meanwhile, 3-(1*H*-indol-3-yl)-3-oxopropanenitrile reacts with the activated carbonyl group of the aldehyde, forming intermediate **(I)** after the elimination of one molecule of H_2O. In the following step, uracil, acting as a nucleophile, reacts with intermediate **(I)** as a Michael acceptor, leading to the formation of intermediate **(II)**. Next, intermediate **(II)** undergoes tautomerization to yield intermediate **(III)**. Then, in intermediate **(III)**, intramolecular cyclization occurs through the attack of the amine group, accompanied by the elimination of one water molecule, leading to the formation of 1,4-dihydropyridine as intermediate **(IV)**. In the last step, intermediate **(IV)** is converted into its corresponding pyridine derivatives *via* a cooperative vinylogous anomeric-based oxidation (CVABO) by losing (H_2) and/or hydrogen peroxide (H_2O_2)[39] (Scheme 3). To further investigate the proposed mechanism, this reaction was also carried out under an argon (Ar) and nitrogen (N_2) atmosphere. The obtained results confirmed the validity of the suggested mechanism based on CVABO.

To evaluate the efficiency of UiO-66(Fe/Zr)–$N(CH_2PO_3H_2)_2$ as a new porous bimetallic catalyst, various organic and inorganic

Table 3 Efficiency of various catalysts in the synthesis of pyrido[2,3-*d*]pyrimidine derivatives

Entry	Catalyst	(mg)	Time (min)	Yield (%)
1	CQDs-N$(CH_2PO_3H_2)_2$ (ref. 28)	10	120	40
2	Piperidine	10 (mol%)	120	30
3	MIL-88B(Fe_2/Co)–N$(CH_2PO_3H_2)_2$ (ref. 17)	10	240	Trace
4	CQDs-N$(CH_2PO_3H_2)_2$/SBA-15 (ref. 49)	10	60	50
5	MIL-88B(Fe_2/Co)-Bnta$[CH_2CO_2H]Br$[18]	10	90	24
6	Et_3N	10 (mol%)	120	40
7	SSA[50]	10	150	30
8	*p*-TSA	10 (mol%)	60	15
9	H_3PO_3	10 (mol%)	75	Trace
10	Uio-66(Fe/Zr)–NH_2 (ref. 44)	10	40	70
11	UiO-66(Fe/Zr)–NH_2 + H_3PO_3	10 (1 : 1)	35	75
12	UiO-66(Fe/Zr)–NH_2 + H_3PO_3 + HCOH	10 (1 : 1:1)	35	75
13	UiO-66(Fe/Zr)–N$(CH_2PO_3H_2)_2$	10	15	85

catalysts, bimetallic MOFs, a simple mixture of H_3PO_3 and UiO-66(Fe/Zr)–NH_2 and a mixture of the three components [UIO-66(Fe/Zr)NH_2 + H_3PO_3 + HCHO] were studied in the reaction of uracil (1 mmol, 0.155 g), 3-(1*H*-indol-3-yl)-3-oxopropanenitrile (1 mmol, 0.184 g) and 4-chlorobenzaldehyde (1 mmol, 0.14 g). The results are shown in Table 3. The utilization of UiO-66(Fe/Zr)–N$(CH_2PO_3H_2)_2$ as a new porous bimetallic catalyst showed the highest efficiency for the synthesis of pyrido[2,3-*d*] pyrimidines. Additionally, the recyclability of the catalyst was investigated in the model reaction, demonstrating that the catalyst could be reused 4 times without a significant loss in efficiency. FT-IR and XRD analyses of the recovered catalyst were conducted, and the results indicated that the catalyst maintained good stability after recovery. According to the obtained results, UiO-66(Fe/Zr)–N$(CH_2PO_3H_2)_2$ is the best catalyst for the synthesis of pyrido[2,3-*d*]pyrimidines (Fig. 8).

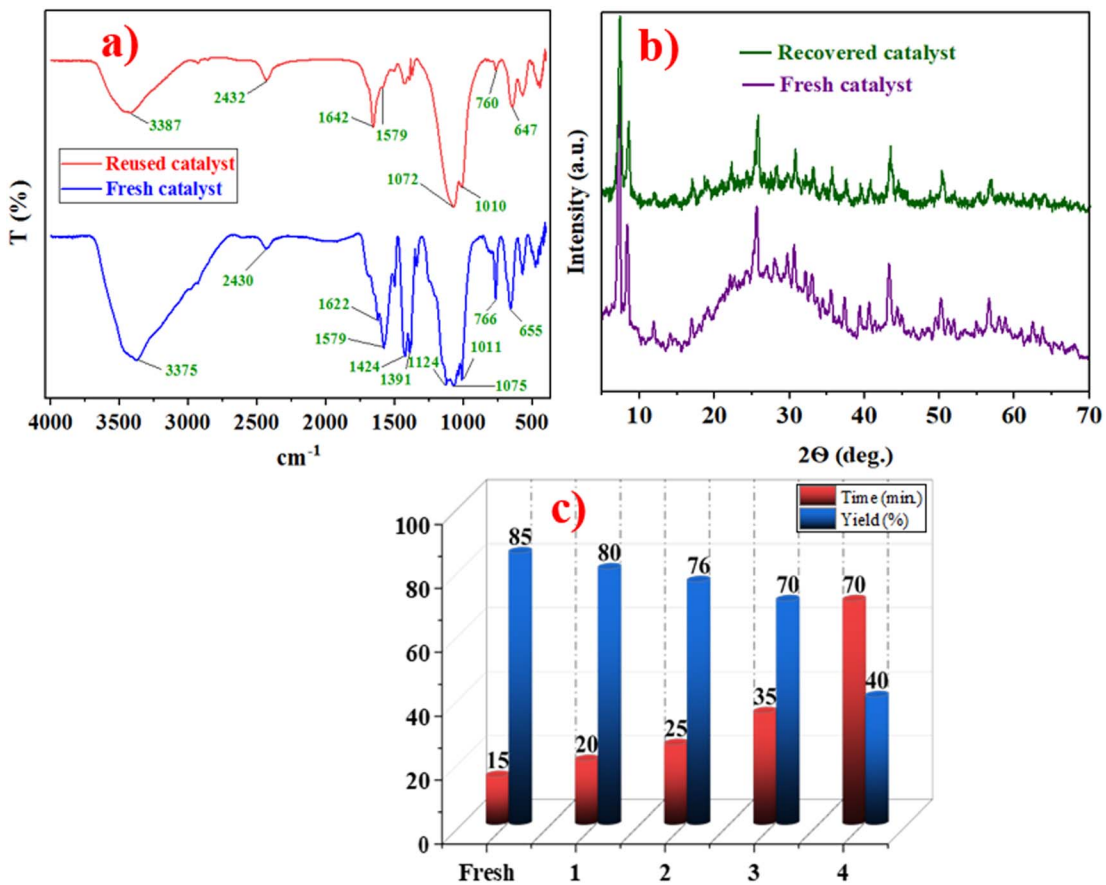

Fig. 8 (a) FT-IR spectra, (b) XRD analysis and (c) recyclability of UiO-66(Fe/Zr)–N$(CH_2PO_3H_2)_2$ for the synthesis of pyrido[2,3-*d*]pyrimidine.

Conclusion

In this study, a bimetallic–organic framework was prepared using iron (Fe) and zirconium (Zr) as metal components. Then, the bimetallic–organic framework was post-modified by incorporating phosphorous acid groups. The combination of two metals and phosphorous acid functional groups in the catalyst architecture simultaneously improved catalytic activity. UiO-66(Fe/Zr)–N($CH_2PO_3H_2$)$_2$ was fully characterized using various techniques. The catalyst was used for the synthesis of pyrido[2,3-*d*]pyrimidine derivatives with indole and uracil skeletons *via* anomeric-based oxidation. Mild and green synthesis conditions, catalyst recoverability and reusability, short reaction times and high product yields are important advantages of this study.

Data availability

ESI,† including spectral data of pyrido[2,3-*d*]pyrimidine derivatives, is freely available and will be provided from the corresponding author upon reasonable request.

Conflicts of interest

The authors declare no competing financial interest.

Acknowledgements

We thank Bu-Ali Sina University for its financial support of this research.

References

1 C. P. Raptopoulou, Metal-organic frameworks: Synthetic methods and potential applications, *Materials*, 2021, **14**, 310.
2 J. Annamalai, P. Murugan, D. Ganapathy, D. Nallaswamy, R. Atchudan, S. Arya, A. Khosla, S. Barathi and A. K. Sundramoorthy, Synthesis of various dimensional metal organic frameworks (MOFs) and their hybrid composites for emerging applications-a review, *Chemosphere*, 2022, **298**, 134184.
3 M. Safaei, M. M. Foroughi, N. Ebrahimpoor, S. Jahani, A. Omidi and M. Khatami, A review on metal-organic frameworks: Synthesis and applications, *TrAC, Trends Anal. Chem.*, 2019, **118**, 401–425.
4 A. Bavykina, N. Kolobov, I. S. Khan, J. A. Bau, A. Ramirez and J. Gascon, Metal-organic frameworks in heterogeneous catalysis: recent progress, new trends, and future perspectives, *Chem. Rev.*, 2020, **120**, 8468–8535.
5 A. Dhakshinamoorthy, Z. Li and H. Garcia, Catalysis and photocatalysis by metal organic frameworks, *Chem. Soc. Rev.*, 2018, **47**, 8134–8172.
6 V. V. E. Butova, M. A. Soldatov, A. A. Guda, K. A. Lomachenko and C. Lamberti, Metal-organic frameworks: structure, properties, methods of synthesis and characterization, *Russ. Chem. Rev.*, 2016, **85**, 280.
7 L. R. Redfern and O. K. Farha, Mechanical properties of metal-organic frameworks, *Chem. Sci.*, 2019, **10**, 10666–10679.
8 S. Zhang, J. Wang, Y. Zhang, J. Ma, L. Huang, S. Yu, L. Chen, G. Song, M. Qiu and X. Wang, Applications of water-stable metal-organic frameworks in the removal of water pollutants: A review, *Environ. Pollut.*, 2021, **291**, 118076.
9 F. Saraci, V. Quezada-Novoa, P. R. Donnarumma and A. J. Howarth, Rare-earth metal-organic frameworks: from structure to applications, *Chem. Soc. Rev.*, 2020, **49**, 7949–7977.
10 S. Lu, L. Liu, H. Demissie, G. An and D. Wang, Design and application of metal-organic frameworks and derivatives as heterogeneous Fenton-like catalysts for organic wastewater treatment: A review, *Environ. Int.*, 2021, **146**, 106273.
11 H. Sepehrmansourie, H. Alamgholiloo, M. A. Zolfigol, N. N. Pesyan and M. M. Rasooll, Nanoarchitecting a Dual Z-Scheme Zr-MOF/Ti-MOF/g-C_3N_4 Heterojunction for Boosting Gomberg-Buchmann-Hey Reactions under Visible Light Conditions, *ACS Sustain. Chem. Eng.*, 2023, **11**, 3182–3193.
12 L. Jiao, Y. Wang, H. L. Jiang and Q. Xu, Metal-organic frameworks as platforms for catalytic applications, *Adv. Mater.*, 2018, **30**, 1703663.
13 V. R. Remya and M. Kurian, Synthesis and catalytic applications of metal-organic frameworks: a review on recent literature, *Int. Nano Lett.*, 2019, **9**, 17–29.
14 L. Chen, H. F. Wang, C. Li and Q. Xu, Bimetallic metal-organic frameworks and their derivatives, *Chem. Sci.*, 2020, **11**, 5369–5403.
15 S. Liu, Y. Qiu, Y. Liu, W. Zhang, Z. Dai, D. Srivastava, A. Kumar, Y. Pan and J. Liu, Recent advances in bimetallic metal-organic frameworks (BMOFs): Synthesis, applications and challenges, *New J. Chem.*, 2022, **46**, 13818–13837.
16 A. Kumari, S. Kaushal and P. P. Singh, Bimetallic metal organic frameworks heterogeneous catalysts: Design, construction, and applications, *Mater. Today Energy*, 2021, **20**, 100667.
17 M. M. Rasooll, H. Sepehrmansourie, M. Zarei, M. A. Zolfigol, M. Hosseinifard and Y. Gu, Catalytic Application of Functionalized Bimetallic–Organic Frameworks with Phosphorous Acid Tags in the Synthesis of Pyrazolo[4, 3-*e*] pyridines, *ACS Omega*, 2023, **8**, 25303–25315.
18 E. Tavakoli, H. Sepehrmansourie, M. A. Zolfigol, A. Khazaei, A. Mohammadzadeh, E. Ghytasranjbar and M. A. As' Habi, Synthesis and Application of Task-Specific Bimetal–Organic Frameworks in the Synthesis of Biological Active Spiro-Oxindoles, *Inorg. Chem.*, 2024, **63**, 5805–5820.
19 D. Sun, F. Sun, X. Deng and Z. Li, Mixed-metal strategy on metal-organic frameworks (MOFs) for functionalities expansion: Co substitution induces aerobic oxidation of cyclohexene over inactive Ni-MOF-74, *Inorg. Chem.*, 2015, **54**, 8639–8643.
20 G. S. More, A. K. Kar and R. Srivastava, Cu–Ce bimetallic metal–organic framework-derived, oxygen vacancy-boosted visible light-active Cu_2O–CeO_2/C heterojunction: An

efficient photocatalyst for the Sonogashira coupling reaction, *Inorg. Chem.*, 2022, **61**, 19010–19021.

21 Y. Hu, J. Zhang, H. Huo, Z. Wang, X. Xu, Y. Yang, K. Lin and R. Fan, One-pot synthesis of bimetallic metal-organic frameworks (MOFs) as acid-base bifunctional catalysts for tandem reaction, *Catal. Sci. Technol.*, 2020, **10**, 315–322.

22 B. Danishyar, H. Sepehrmansourie, H. Ahmadi, M. Zarei, M. A. Zolfigol and M. Hosseinifard, Application of Nanomagnetic Metal–Organic Frameworks in the Green Synthesis of Nicotinonitriles *via* Cooperative Vinylogous Anomeric-Based Oxidation, *ACS Omega*, 2023, **8**, 18479–18490.

23 S. Babaee, H. Sepehrmansourie, M. Zarei, M. A. Zolfigol and M. Hosseinifard, Synthesis of picolinates *via* a cooperative vinylogous anomeric-based oxidation using UiO-66(Zr)–$N(CH_2PO_3H_2)_2$ as a catalyst, *RSC Adv.*, 2023, **13**, 22503–22511.

24 H. Sepehrmansourie, M. Zarei, M. A. Zolfigol, S. Babaee, S. Azizian and S. Rostamnia, Catalytic synthesis of new pyrazolo[3,4-*b*]pyridine *via* a cooperative vinylogous anomeric-based oxidation, *Sci. Rep.*, 2022, **12**, 14145.

25 H. Sepehrmansourie, S. Kalhor, M. Zarei, M. A. Zolfigol and M. Hosseinifard, A convenient catalytic method for preparation of new tetrahydropyrido[2,3-*d*]pyrimidines *via* a cooperative vinylogous anomeric based oxidation, *RSC Adv.*, 2022, **12**, 34282–34292.

26 E. Tavakoli, H. Sepehrmansourie, M. Zarei, M. A. Zolfigol, A. Khazaei and M. Hosseinifard, Applications of novel composite UiO-66-NH_2/Melamine with phosphorous acid tags as a porous and efficient catalyst for the preparation of novel spiro-oxindoles, *New J. Chem.*, 2022, **46**, 19054–19061.

27 S. Kalhor, M. Zarei, M. A. Zolfigol, H. Sepehrmansourie, D. Nematollahi, S. Alizadeh, H. Shi and J. Arjomandi, Anodic electrosynthesis of MIL-53(Al)-$N(CH_2PO_3H_2)_2$ as a mesoporous catalyst for synthesis of novel (*N*-methylpyrrol)-pyrazolo[3,4-*b*]pyridines *via* a cooperative vinylogous anomeric based oxidation, *Sci. Rep.*, 2021, **11**, 19370.

28 M. M. Rasooll, M. Zarei, M. A. Zolfigol, H. Sepehrmansourie, A. Omidi, M. Hasani and Y. Gu, Novel nano-architectured carbon quantum dots (CQDs) with phosphorous acid tags as an efficient catalyst for the synthesis of multisubstituted 4*H*-pyran with indole moieties under mild conditions, *RSC Adv.*, 2021, **11**, 25995–26007.

29 M. Mohammadi Rasooll, Phosphorus acid: As multi-purpose catalysts, *Iran. J. Catal.*, 2022, **12**, 107–113.

30 D. Kumar, S. Sharma, S. Kalra, G. Singh, V. Monga and B. Kumar, Medicinal perspective of indole derivatives: recent developments and structure-activity relationship studies, *Curr. Drug Targets*, 2020, **21**, 864–891.

31 G. Q. Lu, X. Y. Li, D. Wang and F. H. Meng, Design, synthesis and biological evaluation of novel uracil derivatives bearing 1,2,3-triazole moiety as thymidylate synthase (TS) inhibitors and as potential antitumor drugs, *Eur. J. Med. Chem.*, 2019, **171**, 282–296.

32 P. Yadav and K. Shah, An overview on synthetic and pharmaceutical prospective of pyrido[2,3-*d*]pyrimidines scaffold, *Chem. Biol. Drug Des.*, 2021, **97**, 633–648.

33 I. V. Alabugin, L. Kuhn, M. G. Medvedev, N. V. Krivoshchapov, V. A. Vil, I. A. Yaremenko, P. Mehaffy, M. Yarie, A. Terent'ev and M. A. Zolfigol, Stereoelectronic power of oxygen in control of chemical reactivity: the anomeric effect is not alone, *Chem. Soc. Rev.*, 2021, **50**, 10253–10345.

34 I. V. Alabugin, L. Kuhn, N. V. Krivoshchapov, P. Mehaffy and M. G. Medvedev, Anomeric effect, hyperconjugation and electrostatics: Lessons from complexity in a classic stereoelectronic phenomenon, *Chem. Soc. Rev.*, 2021, **50**, 10212–10252.

35 M. Yarie, Catalytic anomeric based oxidation, *Iran. J. Catal.*, 2017, **7**, 85–88.

36 M. Yarie, Spotlight: Catalytic vinylogous anomeric based oxidation (Part I), *Iran. J. Catal.*, 2020, **10**, 79–83.

37 S. Kalhor, M. Zarei, H. Sepehrmansourie, M. A. Zolfigol, H. Shi, J. Wang, J. Arjomandi, M. Hasani and R. Schirhagl, Novel uric acid-based nano organocatalyst with phosphorous acid tags: Application for synthesis of new biologically-interest pyridines with indole moieties *via* a cooperative vinylogous anomeric based oxidation, *Mol. Catal.*, 2021, **507**, 111549.

38 S. Babaee, M. Zarei and M. A. Zolfigol, MOF-Zn-NHC as an efficient *N*-heterocyclic carbene catalyst for aerobic oxidation of aldehydes to their corresponding carboxylic acids *via* a cooperative geminal anomeric based oxidation, *RSC Adv.*, 2021, **11**, 36230–36236.

39 E. Tavakoli, H. Sepehrmansourie, M. Zarei, M. A. Zolfigol, A. Khazaei and M. A. As' Habi, Application of Zr-MOFs based copper complex in synthesis of pyrazolo[3,4-*b*]pyridine-5-carbonitriles *via* anomeric-based oxidation, *Sci. Rep.*, 2023, **13**, 9388.

40 H. Sepehrmansourie, M. Mohammadi Rasooll, M. Zarei, M. A. Zolfigol and Y. Gu, Application of Metal-Organic Frameworks with Sulfonic Acid Tags in the Synthesis of Pyrazolo[3,4-*b*]pyridines *via* a Cooperative Vinylogous Anomeric-Based Oxidation, *Inorg. Chem.*, 2023, **62**, 9217–9229.

41 H. Sepehrmansourie, M. Zarei, M. A. Zolfigol, S. Babaee and S. Rostamnia, Application of novel nanomagnetic metal-organic frameworks as a catalyst for the synthesis of new pyridines and 1,4-dihydropyridines *via* a cooperative vinylogous anomeric based oxidation, *Sci. Rep.*, 2021, **11**, 5279.

42 H. Ahmadi, M. Zarei and M. A. Zolfigol, Catalytic Application of a Novel Basic Alkane-sulfonate Metal-organic Frameworks in the Preparation of Pyrido[2,3-*d*]pyrimidines *via* a Cooperative Vinylogous Anomeric-based Oxidation, *ChemistrySelect*, 2022, **7**, e202202155.

43 M. A. Zolfigol, S. Azizian, M. Torabi, M. Yarie and B. Notash, The importance of non-stoichiometric ratio of reactants in organic synthesis, *J. Chem. Educ.*, 2024, **101**, 877–881.

44 X. Li, P. Liu, X. Niu, K. Ye, L. Ni, D. Du, J. Pan and Y. Lin, Trifunctional Fe-Zr bi-metal-organic frameworks enable high-

performance phosphate ion ratiometric fluorescent detection, *Nanoscale*, 2020, **2**, 19383–19389.

45 U. SuriáBabu, J. BabuáNanubolu and M. SridháraReddy, Rh-catalyzed chemo-, stereo- and regioselective C–H cascade annulation of indolyloxopropanenitriles for pyranoindoles, *Chem. Commun.*, 2023, **9**, 10137–10140.

46 Y. Long, M. Yu, A. M. Ochnik, J. D. Karanjia, S. K. Basnet, A. A. Kebede, L. Kou and S. Wang, Discovery of novel 4-azaaryl-*N*-phenylpyrimidin-2-amine derivatives as potent and selective FLT3 inhibitors for acute myeloid leukaemia with FLT3 mutations, *Eur. J. Med. Chem.*, 2021, **213**, 113215.

47 P. S. Naidu, P. Borah and P. J. Bhuyan, Synthesis of some novel functionalized dihydropyrido [2,3-*d*]pyrimidines *via* an one-pot three-component reaction catalysed by $InCl_3$, *Tetrahedron Lett.*, 2012, **53**, 4015–4017.

48 M. Mamaghani, M. Sheykhan, M. Sadeghpour and F. Tavakoli, An expeditious one-pot synthesis of novel bioactive indole-substituted pyrido[2,3-*d*]pyrimidines using Fe_3O_4@SiO_2-supported ionic liquid nanocatalyst, *Monatsh. Chem.*, 2018, **149**, 1437–1446.

49 M. M. Rasooll, H. Sepehrmansourie, M. Zarei, M. A. Zolfigol and S. Rostamnia, Phosphonic acid tagged carbon quantum dots encapsulated in SBA-15 as a novel catalyst for the preparation of *N*-heterocycles with pyrazolo, barbituric acid and indole moieties, *Sci. Rep.*, 2022, **12**, 20812.

50 M. A. Zolfigol, Silica sulfuric acid/$NaNO_2$ as a novel heterogeneous system for production of thionitrites and disulfides under mild conditions, *Tetrahedron*, 2001, **57**, 9509–9511.